International Journal of Environmental Science and Technology
https://doi.org/10.1007/s13762-019-02593-z

ORIGINAL PAPER

Fe-modified hydrochar from orange peel as adsorbent of food colorant Brilliant Black: process optimization and kinetic studies

F. N. Çatlıoğlu[1] · S. Akay[1] · B. Gözmen[2] · E. Turunc[3] · I. Anastopoulos[4] · B. Kayan[1] · D. Kalderis[5]

Received: 20 March 2019 / Revised: 10 November 2019 / Accepted: 15 November 2019

Abstract

The main aims of this work were to produce and characterize Fe-modified hydrochar from orange peel waste, optimize the adsorption through response surface methodology, investigate the role of treatment time, dye concentration, adsorbent dose and temperature, and determine the dominant mechanisms through kinetics analysis. Orange peel waste was hydrothermally carbonized at 200 °C for 8 h, and the hydrochar was embedded with magnetite nanoparticles. The composite adsorbent was characterized through spectrometric and surface analytical methods. Subsequently, analysis of variance was used to design the experimental runs, propose a polynomial equation describing the adsorption process and finally optimize the adsorption conditions. The results indicated that 99% removal can be theoretically achieved at the following conditions: dye initial concentration of 6.08 mg/L, treatment time of 26.30 min, temperature of 44.79 °C and adsorbent concentration of 2.27 g/L. The dominant factors were the dye and adsorbent concentration, whereas time and temperature variations had a much lesser impact. Among examined models, the Langmuir model showed a better match to the experimental data. The maximum monolayer adsorption capacity was determined as 10.49 mg/g. The mechanism of interaction was largely based on surface chemisorption between the dye and adsorbent. Fe-modified hydrochar exhibited a positive adsorption behavior, and it was shown that a new valorization option for orange peel waste is available. This option may follow other valorization pathways, such as isolation of biologically active molecules, therefore offering a complete solution to this type of waste.

Editorial responsibility: M. Abbaspour.

✉ D. Kalderis
kalderis@hmu.gr

[1] Department of Chemistry, Arts and Science Faculty, Aksaray University, 68100 Aksaray, Turkey

[2] Department of Chemistry, Arts and Science Faculty, Mersin University, 33342 Mersin, Turkey

[3] Advanced Technology of Education, Research and Application Center, Mersin University, 33343 Mersin, Turkey

[4] Department of Chemistry, University of Cyprus, P.O. Box 20537, 1678 Nicosia, Cyprus

[5] Department of Electronic Engineering, School of Engineering, Hellenic Mediterranean University, 73100 Chania, Crete, Greece

Published online: 26 November 2019

Graphic abstract

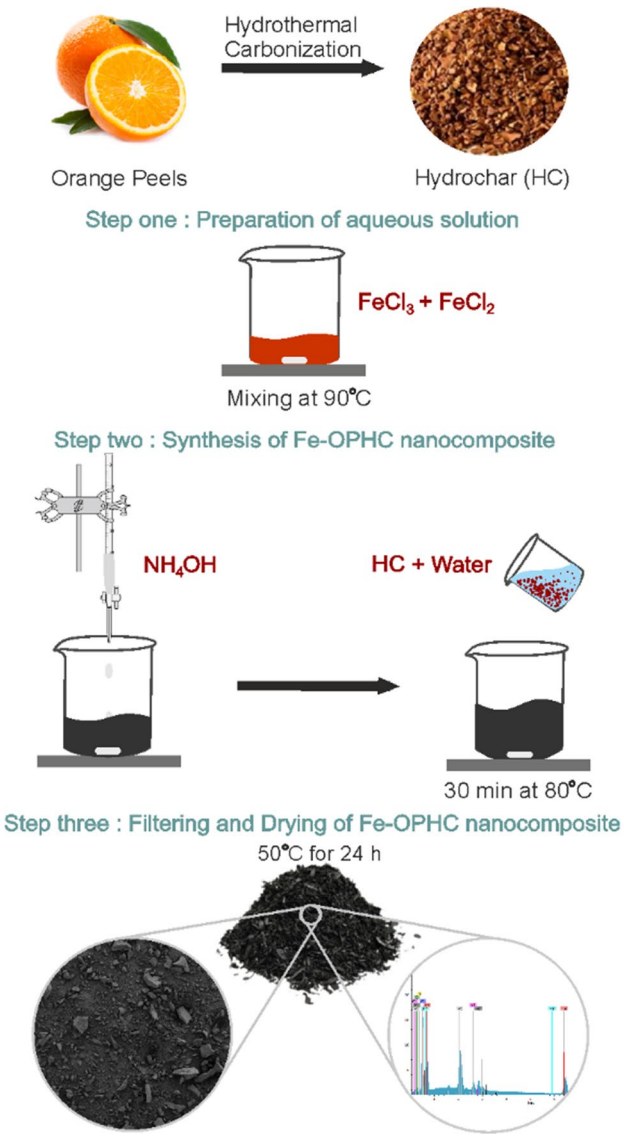

Keywords Adsorption · Agricultural waste · Hydrochar · Hydrothermal carbonization · Orange peel waste

Introduction

The food industry often makes use of synthetic or natural dyes to adjust the color of a wide range of products. These additives may correct or even enhance the natural color of foodstuff, whereas sometimes they make food more appealing and appetizing. Back in the nineteenth century, there was a rapid increase in the unregulated use of food colorants, the toxicity of which was not tested. Since then, a number of poisoning incidents and the development of analytical methods led to the screening of synthetic food colorants and the subsequent development of regulations.

Recent studies by the European Food Safety Authority (EFSA) have highlighted the health risks of food azo dyes, the main ones being children hyperactivity, allergies and development of intolerances. This is the case of food dyes such as E122, E123 and E129, whose application remains debatable in several European countries (European Food Safety Authority 2015). Similarly, Brilliant Black BN (E151) is an azo dye commonly used in food decorations, desserts, sweets, ice creams and soft drinks; however, its use has been forbidden in the USA and Japan. As a Priority 3 food additive, its use is closely monitored by the EFSA (European Food Safety Authority 2010). The effects of azo dyes in human health have

been well studied and published in excellent review articles (Rovira and Domingo 2019; Holkar et al. 2016).

There are various methods (chemical, biological and physical) that are widely used for the elimination of dyes from wastewater including adsorption (Deepa et al. 2018), ion exchange, coagulation/flocculation, chemical oxidation, membrane filtration, electrochemical treatment, photocatalysis (Gnanasekaran et al. 2019; Saravanan et al. 2018; Qin et al. 2017), aerobic and anaerobic degradation and so on (Zhou et al. 2019). Compared to other methods, adsorption is often advantageous for water reuse in terms of flexibility and simplicity of design, ease of operation, initial cost and insensitivity to toxic pollutants (Sivarajasekar and Baskar 2015). Some examples of adsorbents for various pollutants removal are: starch/poly(alginic acid-cl-acrylamide) nanohydrogel (Sharma et al. 2017), Amberlite Ira-938 resin (Naushad et al. 2016a), acidic cation-exchange resin Amberlite IR-120 (Naushad and Al-Othman 2015), Amberlite IRA-400 resin (Naushad et al. 2016b), modified by graft copolymerization *Hibiscus cannabinus* fiber (Sharma et al. 2015), activated carbons prepared from peanut shell (Al-Othman et al. 2012), starch/SnO_2 nanocomposite (Naushad et al. 2016c), nickel ferrite-modified mesoporous carbon (Naushad et al. 2017), microalgae (Daneshvar et al. 2017) and surfactant-assisted nanocomposite cation exchanger (Naushad 2014). Among examined materials, orange peels have received increased attention, because they are available in large quantities at low or no cost and in most orange processing areas a sustainable exploitation plan is absent (Anastopoulos and Kyzas 2014).

Hydrothermal carbonization (HTC) is a closed reactor process, where biomass is converted to an added-value material called hydrochar, in the presence of water at temperatures in the range of 150–350 °C (subcritical water region). The use of subcritical water (with or without oxidants) has been established as a wastewater treatment process in the past; however, it has attracted attention lately as a biomass conversion technology for the production of hydrochar. Compared to conventional pyrolysis, hydrothermal carbonization offers the advantages of treating wet biomass and using lower treatment temperatures. Hydrochars have been tested mostly as fuels, independently or in combination with other materials (Román et al. 2015). Among others, Guo et al. (2016a) concluded that the percentage of initial moisture has a significant effect on hydrochar yield, whereas the higher heating value and carbon content are strongly dependent on the properties of the feedstock. Wang et al. (2018) and Libra et al. (2011) have published in-depth reviews of the mechanisms involved in hydrothermal carbonization and their relative importance. Other promising hydrochar applications include its use as a catalyst for chemical reactions, as a substrate component for soilless growth of plants, as a precursor for supercapacitor electrodes and as a soil amendment (Román et al. 2015; Wang et al. 2018; Libra et al. 2011; Khataee et al. 2017). However, due to the reduced degree of carbonization and condensation achieved through the hydrothermal conversion of biomass, hydrochars have relatively low medium-term stability in soil (Libra et al. 2011). Therefore, their efficiency in soil-related applications requires longer-term studies.

Typically, hydrochars have a low surface area, often below 100 m^2/g; therefore, they are not the best possible candidates for adsorption processes that rely on the surface area and total pore volume (Khataee et al. 2017; Kalderis et al. 2014). The published literature where hydrochars were used in adsorption studies without any modification steps is limited. Han et al. (2017) compared hydrochars and biochars prepared from swine solids and poultry litter for the adsorption of Cd^{2+} and Sb^{3+}. Overall, the biochar obtained from conventional pyrolysis at 450 °C was found to be more suitable for the immobilization of these metal ions, compared to the hydrochars. Low surface area, unmodified hydrochars from banana peel performed better when tested against Pb^{2+} solutions. Zhou et al. (2017) achieved adsorption capacities up to 359 mg/g which they assigned to the increased content of oxygen-containing groups on the hydrochar surface. The decisive role of the surface functional groups was also confirmed by Takaya et al. (2016) who investigated the adsorption of phosphate and ammonium on various low surface area hydrochars. With respect to organic contaminants, unmodified hydrochars have been used successfully for the adsorption of *p*-nitrophenol (Román et al. 2016) and model dye substance (Parshetti et al. 2014). These studies come to an agreement that multiple mechanisms, such as H-bonding, electrostatic interactions and hydrophobicity, significantly affect the adsorption process.

Researchers have focused on developing methods to improve the adsorption behavior of hydrochars. Similar to other carbonaceous adsorbents, hydrochars can be chemically or physically activated. Quesada-Plata et al. employed coconut shells, almond shells, hemp residues and sawdust to prepare chars through H_3PO_4-assisted hydrothermal treatment followed by a carbonization step. Through this protocol, they obtained higher solid yields and activated hydrochars with surface area exceeding 2000 m^2/g (Quesada-Plata et al. 2016). Using KOH, K_2CO_3 or NaOH to activate hydrochars not only leads to higher surface area materials but also increases the oxygen-containing functional groups on the surface. This has been demonstrated on contaminants, such as lead (Zhou et al. 2017), phosphate and ammonium (Takaya et al. 2016) and methylene blue (Unur 2013). Physical activation through N_2 or CO_2 is also an alternative pathway to improve the adsorption behavior of hydrochars (Fang et al. 2016).

The modification of the adsorbent surface with Fe and other metals is gradually gaining attention. The formation

of Fe/char composites improves the interaction between the surface and the contaminant, whereas it allows for quick and simple magnetic separation of the spent adsorbent after treatment. Tang et al. impregnated hydrochars prepared from biogas residues with Ni/Fe and applied the composite to adsorb Pb^{2+} from synthetic wastewaters. The presence of Ni/Fe nanoparticles induced Pb^{2+} to move toward the surface, leading to a near-complete removal of the metal ion after 90 min of treatment (Tang et al. 2016). Magnetite (Fe_3O_4) nanoparticles have the advantages of high surface area and low mass transfer resistance (Moeser et al. 2002). In our previous study, hydrochars from coffee waste were loaded with Fe_3O_4 nanoparticles and the composite was tested for the removal of Acid Red 17 from wastewaters (Khataee et al. 2017). Aided by ultrasonic irradiation, 99.9% removal was achieved when 1 g/L and 10 mg/L of adsorbent and Acid Red 17 concentration were used, respectively. The reusability tests indicated that the hydrochar composite can be used for multiple adsorption–desorption cycles. Based on the knowledge obtained from our previous studies and the increasing demand for waste-derived adsorbents, in the present work the hydrothermal carbonization of orange peel waste was investigated. The logic behind this work was to advance a solid waste management option based on the exploitation of a widely available agricultural waste, whereas at the same time it was to obtain a novel product of added value. Therefore, the main objectives were: (1) to produce and characterize Fe-modified hydrochar from orange peel waste, (2) to optimize the adsorption of food colorant Brilliant Black BN through response surface methodology, (3) to examine the role of treatment time, dye concentration, adsorbent dose and temperature on the process and (4) to determine the dominant mechanisms through kinetics analysis. This work was partly performed at the Hellenic Mediterranean University in Greece (adsorbent preparation and characterization) and partly at the University of Aksaray in Turkey (adsorbent characterization and adsorption studies), between January and July 2018.

Materials and methods

Materials

Brilliant Black BN (tetrasodium-4-acetamido-5-hydroxy-6-[7-sulfonato-4-(4-sulfonatophenylazo)-1 naphthylazo]-1,7-naphthalene-disulfonate, chemical formula $C_{28}H_{17}N_5Na_4O_{14}S_4$) is an azo dye used as food colorant under the code E151 (Sigma-Aldrich, Germany). Its structure is shown in Fig. 1. Brilliant Black BN will be referred to as BB thereof.

At first, a concentrated solution of 50 mg/L was prepared. Each experimental solution was produced at the desired concentration (according to the Box–Behnken design) by dilution of the concentrated solution with ultra-pure water. All necessary reagents for the deposition of Fe_3O_4 particles on the hydrochar surface were of analytical grade (Merck, Germany).

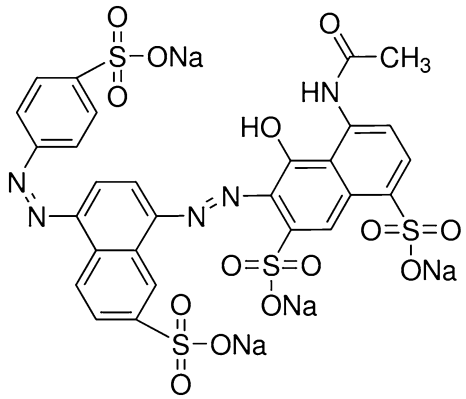

Fig. 1 Molecular structure of Brilliant Black BN

Several oranges (*Citrus sinensis*) were washed and peeled. The peels were homogenized at a conventional blender until a uniform paste was obtained (~70% moisture). Moisture was reduced to ~50% by drying the past at 80 °C for 2 h. The paste, referred to as OP from now on, was stored at 4 °C until further analyses and use.

Production of orange peel hydrochar (OPHC)

A detailed account of the experimental procedure for the production of hydrochar is provided in Kalderis et al. 2014. In brief, type 316 stainless steel vessels (~25 ml capacity, Swagelok Company, USA) were filled with 20 g of OP paste. No additional water or any other reagents were used. Within the steel vessel, sufficient headspace was allowed to avoid a buildup in pressure due to biomass expansion and ensure operational safety.

A laboratory oven (heated at the required temperature) was used for the hydrothermal carbonization. Experimental zero time was considered the time the vessels were entering the oven. Initial HTC runs were carried out at 150, 200 °C and times of 2, 8, 16 and 24 h. At the end of treatment, each vessel was removed from the oven and quickly cooled down using an ice bath. The resultant hydrochars were recovered by filtration, washed first with acetone and then with distilled water until pH 7 was reached in the filtrate. The samples were then vacuum dried and finally stored in airtight glass containers at room temperature. It has been established that biomass carbonization increases with time, whereas the quantities of surface oxygen groups diminish at treatment times that exceed 12 h (Libra et al. 2011; Parshetti et al. 2014). Since the target application was adsorption, it was

decided to use the sample prepared at 200 °C and 8 h residence time for the preparation of the Fe-modified adsorbent and the subsequent adsorption tests. For reproducibility reasons, at each set of conditions (temperature–treatment time) triplicate runs were performed.

The yield of hydrochar (on a dry basis) was determined as follows:

$$\text{Yield}(\%) = \frac{m_{\text{hydrochar}}}{m_{\text{biomass}}} \times 100 \quad (1)$$

where $m_{\text{hydrochar}}$ is the weight of the hydrochar and m_{biomass} is the initial biomass weight.

The pH, electrical conductivity, ash content and main element (C, H, N, S, Mg, Mn, Ca, K) content were determined through the protocols described in the European Biochar Certificate (European Biochar Foundation (EBC) 2018). The oxygen content was calculated by difference, according to Eq. 2:

$$\text{O}(\%) = 100 - \text{C}(\%) - \text{H}(\%) - \text{N}(\%) - \text{S}(\%) - \text{ash content}(\%). \quad (2)$$

Synthesis of Fe-modified hydrochar (Fe-OPHC)

Fe-OPHC was synthesized through deposition of magnetite (Fe_3O_4) nanoparticles on the hydrochar surface, in alkaline conditions. The procedure is described in detail in Kamboh and Yilmaz (2013) and is summarized as follows. $FeCl_3{\cdot}6H_2O$ (13.32 g), $FeCl_2{\cdot}4H_2O$ (19.88 g), HCl (5 mL–5 M), ultra-pure water (40 mL) and ethanol (5 mL) were added in a 100-mL flask followed by gentle heating until the iron salts were thoroughly dissolved. Hydrochar (1 g) was then added in 30 mL of this solution, and the slurry was further stirred for 2 h at room temperature. The slurry was then vacuum filtered, washed with distilled water and transferred to a flask with 10 mL of 1 M ammonia solution. After a further 2 h of stirring, the Fe_3O_4–hydrochar composite was recovered by magnet, washed to neutral pH with distilled water, dried under vacuum at 60 °C for 24 h and finally stored for further use. The main reaction involved in the preparation of magnetite can be seen below:

$$Fe^{2+} + 2Fe^{3+} + 8OH^- \rightarrow Fe_3O_4 + 4H_2O \quad (3)$$

The exact mechanisms involved in the precipitation and all the phase transformations are described in detail elsewhere (Ahn et al. 2012).

Characterization of OPHC and Fe-OPHC

Dynamic light scattering (DLS) was employed to measure the average hydrodynamic diameter of OPHC. Hydrochar particles were dispersed in deionized water with Sigma 3–30 K model ultrasound equipment, and the measurement was performed at 25 °C, using a Malvern 2000 Zetasizer Nano ZS instrument.

The Fourier transform infrared (FTIR) spectra of OPHC, Fe-OPHC and dye-loaded Fe-OPHC were obtained by using a PerkinElmer IR spectrophotometer (USA). Field emission scanning electron microscopy coupled with energy-dispersive X-ray spectrometry (FE-SEM–EDS) was performed on the same samples using a Quantax instrument (Bruker, USA).

The surface area and pore structure of orange peel powder, OPHC and Fe-OPHC, were investigated through nitrogen adsorption at 77 K using a Micromeritics Gemini VII (2390t). A Zeiss Supra 55 field emission microscope was used to record scanning electron microscopy (SEM) images of OPHC and Fe-OPHC (before and after dye adsorption).

BB batch adsorption study

The adsorption runs were carried out in agreement with the procedure reported in Bagheri et al. 2017. BB solutions with concentrations ranging from 5 to 25 mg/L were used, and appropriate quantities of Fe-OPHC were added. The mixtures were stirred in an ultrasonic bath at the predetermined times and temperatures (conforming to the Box–Behnken design—Table 2). The desired experimental temperature was controlled through a thermocouple fitted in a water bath. After treatment, Fe-OPHC was removed by magnet and the residual BB concentration was measured in a UV–Vis spectrophotometer at a wavelength of 575 nm. The dye adsorption percentage was determined according to the equation below:

$$\text{Adsorption}\,\% = \frac{C_0 - C_e}{C_0} \times 100 \quad (4)$$

where C_0 and C_e are the starting and equilibrium concentration of BB in mg/L, respectively. It has been well established that the use of ultrasonic irradiation in adsorption leads to improved adsorption efficiencies, through a series of accelerated chemical reactions and mass transfer on the adsorbent surface (Khataee et al. 2017; Bagheri et al. 2017).

Study of adsorption kinetics

The kinetics of the process were studied to gain an insight of the mechanisms of interaction between Fe-OPHC and BB. Therefore, 0.125 g of Fe-HC and 10 mg/L BB solutions were used. The solutions were continually stirred at the required temperatures allowing contact times that ranged between 1 and 30 min. They were then filtered, and the filtrate was stored at 4 °C for residual BB analysis. The experimental

adsorption value per unit weight of adsorbent (q_t) was determined as follows:

$$\text{Adsorption capacity}\left(\frac{\text{mg}}{\text{g}}\right) = \frac{(C_0 - C_e)V}{m} \quad (5)$$

where V is the volume of the BB solution, C_0 and C_e are the initial and equilibrium concentrations of BB, respectively, and m is the dry weight of the adsorbent. Consequently, the data were fitted into the Freundlich and Langmuir isotherms to examine the dye–adsorbent interactions in more detail.

Optimization of BB adsorption by response surface methodology

The removal efficiency of Fe-OPHC was determined using a Box–Behnken experimental design (BBD), and statistical analysis of the results was performed with response surface methodology (RSM). Experimental designs such as the BBD lead to the optimization of treatment parameters while minimizing the number of runs required. This is particularly important in cases where experimental conditions and/or the availability of materials restrict the quantity of the composite adsorbent that can be produced. The software Design Expert (8.0.6; Stat-Ease Inc., Minneapolis, USA) was used for the experimental design, data evaluation and response surface model. The BBD allocated three levels (− 1, 0, + 1) to each independent variable, which yielded a total number of 29 experimental runs (Table 2), on the basis of the following equation:

$$N = 2k(k-1) + cp \quad (6)$$

where k is the number of factors and cp corresponds to the number of the central points.

The central point was replicated three times (experiments 25–29) to determine the experimental error. The initial dye concentration (X_1 5, 15, 25 mg/L), adsorption time (X_2 10, 35, 60 min), temperature (X_3 25, 35, 45 °C) and Fe-OPHC concentration (X_4 0.5, 1.5, 2.5 g/L) were the independent variables. The regression equation that formed the response surface model was given by:

$$Y = \beta_0 + \sum_{j=1}^{k} \beta_j X_j + \sum_{j=1}^{k} \beta_{jj} X_j^2 + \sum \sum_{i<j} \beta_{ji} X_i X_j + \varepsilon \quad (7)$$

where Y is the predicted response (adsorption %); X_i and X_j were the independent coded variables ($i \neq j$, $k = 3$); and β_0, β_j, β_{ji} and β_{jj} correspond to the regression coefficients for intercept, linearity, interaction and quadratic, respectively. k is the number of variables, and ε is the residual error.

The influence of each binary and quadratic term on the response Y was determined by analysis of variance (ANOVA) methodology. Three-dimensional (3D) surface plots were plotted while holding a variable constant in the quadratic model. To validate the proposed model, the experimental and predicted removal efficiencies were compared (Table 3). The R^2 and adjusted R^2 coefficient values correlated the experimental to the theoretical results. Pareto chart analysis was employed to determine the influence of each variable with linear and quadratic relation on the response. Finally, the optimal treatment conditions for maximum BB removal were proposed.

Results and discussion

Characterization of OPHC and Fe-OPHC composite

It is fundamental to determine the basic physical and chemical properties of OPHC, since most of these remain the same in the Fe-OPHC composite. Table 1 shows the chemical and physical properties of orange peel and OPHC. The pH was

Table 1 Properties of orange peel and OPHC[a]

	Units	OP (feedstock)	OP hydrochar
pH		4.64	4.71
Yield	%	–	44.3
Electrical conductivity	µS/cm	–	2330
C	%	44.1	66.2
H	%	5.97	5.22
N	%	0.98	1.23
S	%	0.053	0.049
Ash content	%	4.58	6.34
O[b]	%	44.31	20.96
Mg	mg/kg	1305	1110
K	mg/kg	12,790	11,565
Ca	mg/kg	13,360	10,260
Mn	mg/kg	7.58	5.53
Fe	mg/kg	–	315
Cu	mg/kg	–	23.3
P	mg/kg	–	210
Zn	mg/kg	–	75.4
Atomic O/C		–	0.47
Atomic H/C		–	0.94
Particle size distribution			
> 2 mm			34.3
1–2 mm			22.8
500–1 mm			18
250–500 µm			13.5
< 250 µm			11.4
Coarseness index (CI)	%		57.1

[a]Average values are reported, $n = 3$. In all cases, the relative standard deviation was ≤ 11%

[b]Calculated by difference

on the acidic range, typical for most hydrochars due to the production of organic acids during HTC (Libra et al. 2011; Reza et al. 2014). The yield of 44.3% is within the typical range for hydrochar yields (40–80%)—it has been established that these are directly correlated with temperature (Quesada-Plata et al. 2016). The atomic H/C and O/C ratios are an indication of the degree of aromaticity and polarity of carbonaceous products. As the H/C value decreases, so does the degree of aromaticity, whereas a high O/C value indicates a surface of high polarity. The H/C and O/C values of OPHC are similar to values reported in the literature (Simsir et al. 2017). They indicate a product of non-condensed aromatic ring structure and average stability under environmental weathering but with a relatively high content of polar groups.

The results of the dynamic light scattering analysis of OPHC are presented in Fig. 2. A monomodal particle size distribution can be observed, at an average value of 25.05 nm. The SEM images of the external surfaces of samples (OPHC, Fe-OPHC before and after dye adsorption) are shown in Fig. 3. OPHC has an amorphous and irregular appearance (Fig. 3a), typically observed in hydrochars (Reza et al. 2014), whereas after Fe_3O_4 deposition the surface becomes more homogeneous (Fig. 3b). At a higher resolution, the Fe_3O_4 particles can be observed as individual, spherical particles, with diameters in the range of 22–50 nm (Fig. 3c). Aliramaji et al. (2015) prepared pure magnetite nanoparticles using the same $FeCl_3/FeCl_2$ co-precipitation method. They reported Fe_3O_4 nanoparticles in the range of 5–30 nm, whereas their SEM images appeared practically the same as the ones shown here (Aliramaji et al. 2015). Furthermore, these observations come in good agreement with SEM images and particle diameter values obtained in our earlier studies, where Fe_3O_4 was deposited on sporopollenin and biochar (Kulaksiz et al. 2017; Şener et al. 2016).

FE-SEM–EDS analysis verified the presence of Fe on the OPHC surface. A comparison of Fig. 4a, b showed the emergence of two clear peaks at 0.7 and 6.5 keV that corresponded to Fe^{2+} and Fe^{3+}, respectively. The percentage of Fe on the adsorbent was 53.1%.

The low surface area of OPHC (6.3 m^2/g) was the result of pressure buildup within the HTC vessel which restricted the development of an extensive porous network. Incomplete carbonization and the existence of disorganized matter further restrain the development of a porous structure (Fernandez et al. 2015). This value comes in good agreement to earlier works where hydrochars were produced from various precursors (Zhou et al. 2017; Román et al. 2016). The deposition of magnetite particles raised the surface area to 72.5 m^2/g, in good agreement with an earlier study where magnetite nanoparticles were embedded on various biomass precursors (Guo et al. 2016b). For pore size calculations, the Barrett–Joyner–Halenda (BJH) methodology (adsorption) provides more accurate results compared to the BET methodology (De Lange et al. 2014). The average pore width remained practically the same between OPHC (5.2 nm) and Fe-OPHC (7 nm).

Figure 5 shows the N_2 adsorption–desorption isotherm for Fe-OPHC. According to the IUPAC classification, this is a typical example of type II isotherm, indicating an essentially non-porous or macroporous material (Parshetti et al. 2014). This may account for the low surface area of the adsorbent. Type II isotherms represent a combination of monolayer and multilayer adsorption. In this case, the monolayer adsorption ended quite early at a p/p_o value of 0.11 (see arrow), and then, the multilayer adsorption commenced (linear middle part of isotherm). Moreover, the Fe-OPHC isotherm resembled a H3 hysteresis loop, indicating an adsorbent with a very wide pore size distribution, whereas the shape of the loop suggested the presence of non-rigid aggregates

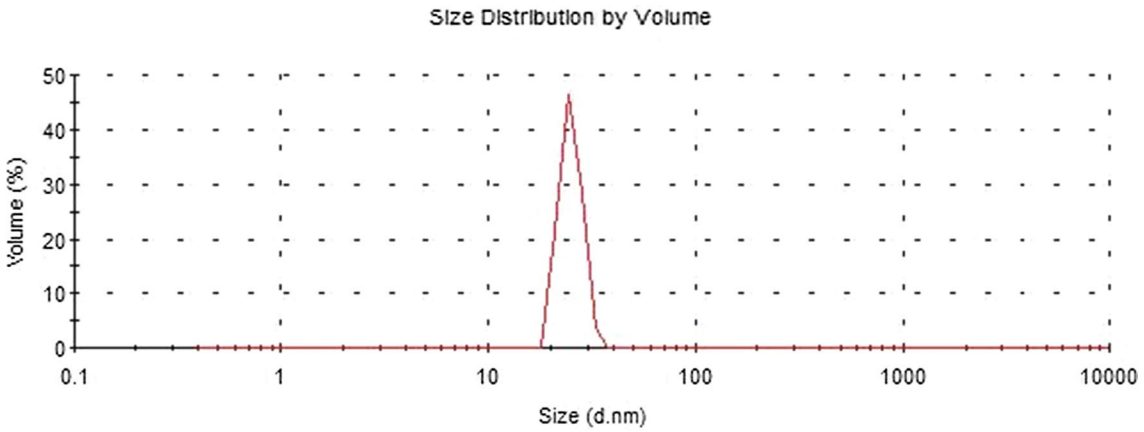

Fig. 2 DLS results for orange peel hydrochar

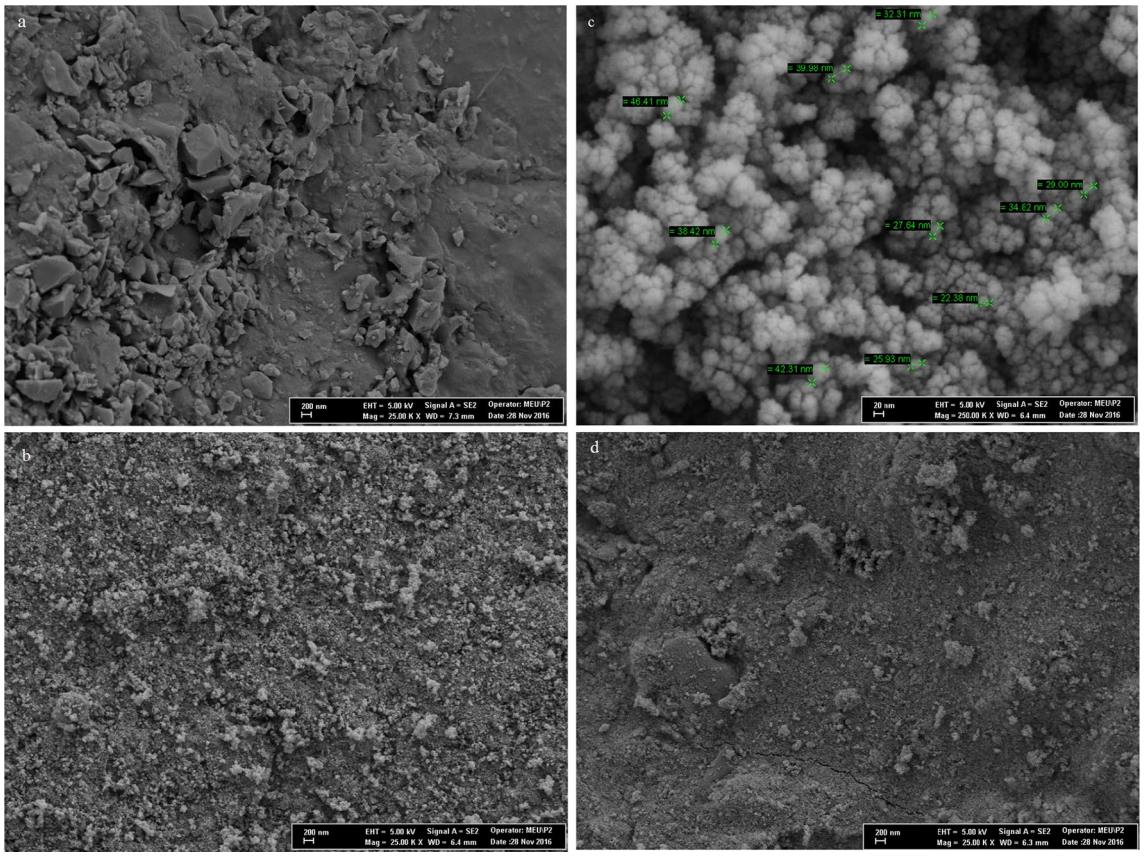

Fig. 3 SEM images of **a** OPHC, **b** and **c** Fe-OPHC and **d** Fe-OPHC after treatment

of plate-like particles or assemblages of slit-shaped pores (Thommes 2010).

The FTIR spectra of orange peel, Fe-OPHC and Fe-OPHC with BB adsorbed, are shown in Fig. 6. Several bands can be identified in the original feedstock due to the stretching and bending vibrations of a wide number of groups. During the hydrothermal carbonization of orange peel, the polysaccharide character of the precursor was lost, as indicated by the disappearance of the intense peaks at ~ 1017 cm^{-1} and 1600–1700 cm^{-1} which correspond to the carboxylic and carboxylate groups, respectively (Fig. 6a, b) (Fernandez et al. 2015). Similarly, the broad band at 3200–3300 cm^{-1} due to the stretching vibration of –OH groups was reduced considerably due to the dehydration stage of the HTC process. The high complexity of the HTC reactions and their products has been thoroughly explained in earlier studies (Libra et al. 2011).

The two washing steps involved in the preparation of the Fe-OPHC composite removed water-soluble products to a large extent. As a result, the FTIR spectrum of the Fe-OPHC composite showed a smaller number of peaks compared to the spectrum of OPHC. The formation of Fe_3O_4 particles on the hydrochar surface was confirmed by the presence of the sharp band at ~ 600 cm^{-1}, which typically corresponds to Fe–O bond deformations. Their absence and formation are clearly shown in Fig. 6a, b, respectively.

There were distinct differences between the spectra of Fe-OPHC and Fe-OPHC with the dye adsorbed, which provided an insight on the functional moieties that participated in the adsorption process (Fig. 6b, c. The broad band at 3200–3300 was intensified, indicating the participation of –OH in adsorption. The band at 1000–1100 cm^{-1} included two peaks (at 1028 and ~ 1045 cm^{-1}) which are assigned to the ether linkage group –C–O–C–and the stretching vibration of the C–O bond in the $–CH_2–OH$ group, respectively. These were enhanced considerably in the spectra of Fe-OPHC (dye adsorbed), suggesting the participation of these groups in adsorption. The band at ~ 1640 cm^{-1} corresponded to the –C=O carbonyl group, slightly shifted at a lower frequency compared to the typical stretching vibration of this group, indicating some degree of conjugation. The weak band 1411 cm^{-1} is typical of the –C=C– stretching vibration and was intensified and shifted (1401 cm^{-1}) during adsorption. These observations suggest a considerable degree of chemisorption between BB and Fe-OPHC.

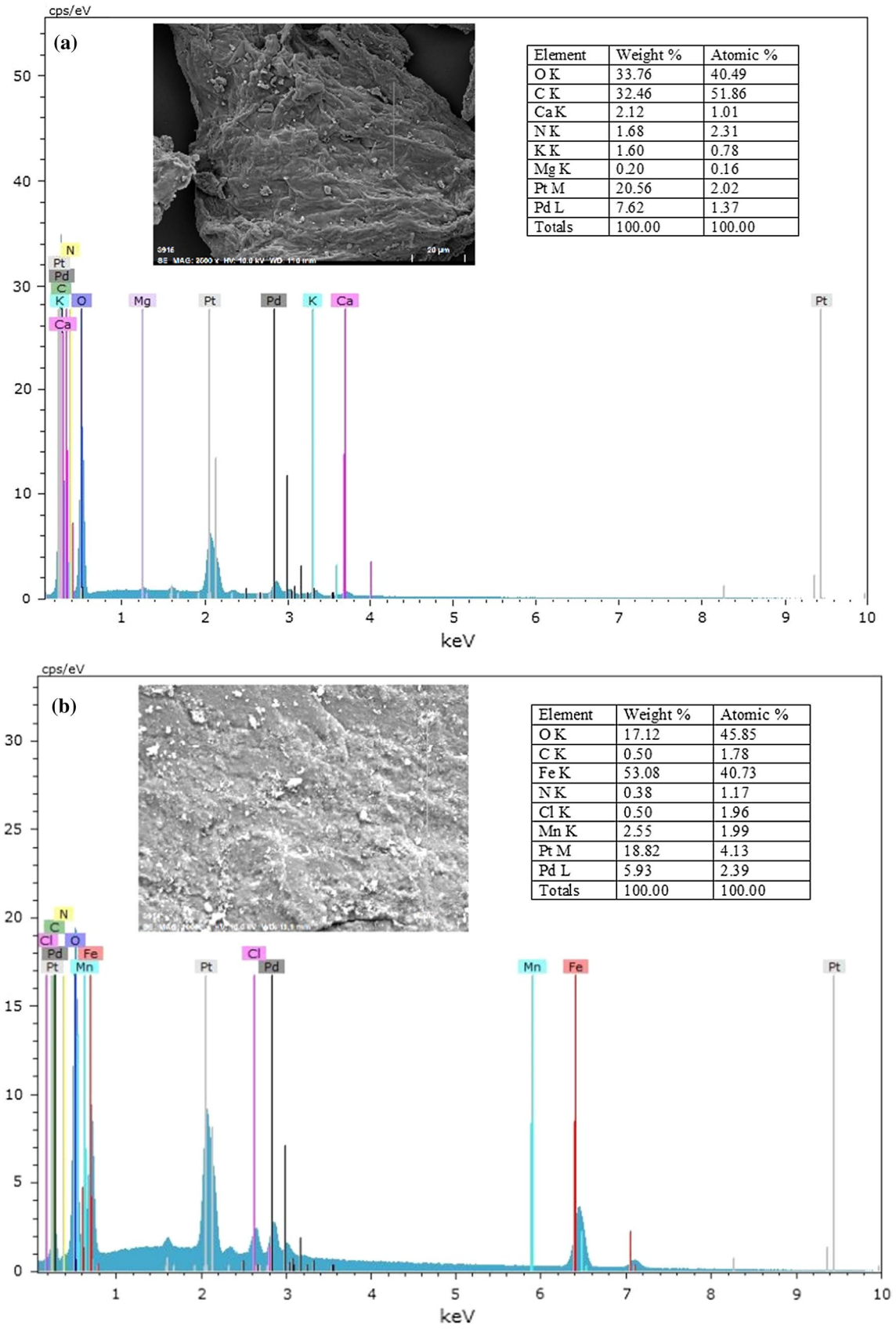

Fig. 4 FE-SEM–EDS analysis of **a** OPHC and **b** Fe-OPHC

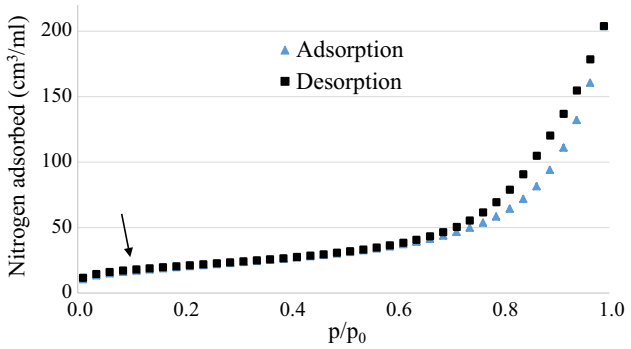

Fig. 5 N_2 adsorption/desorption isotherm of Fe-OPHC

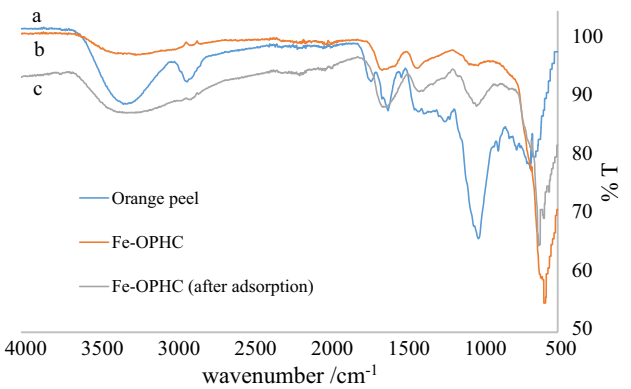

Fig. 6 FTIR spectra of **a** orange peel, **b** Fe-OPHC and **c** Fe-OPHC with adsorbed dye

BB adsorption on Fe-OPHC

The experimental and the predicted values for adsorption % are presented in Table 2. The experimental adsorption values were fitted into polynomial Eq. 7 described earlier. After elimination of insignificant variables and their interactions, the following equation was derived, which mathematically describes the adsorption of BB on Fe-OPHC:

$$\begin{aligned}\text{Adsorption } \% = {} & 67.20 - 15.83X_1 + 2.83X_2 + 3.00X_3 \\ & + 36.83X_4 + 0.50X_1X_2 - 1.25X_1X_4 \\ & - 5.18X_1^2 - 1.93X_2^2 - 1.43X_3^2 - 11.68X_4^2.\end{aligned} \quad (8)$$

There was a high level of agreement among the experimental adsorption % values and those estimated by Eq. 8. Furthermore, the correlation coefficient (R^2) was determined as 98.6%, thus confirming the reliability of the model. The optimum BB adsorption of 98% was achieved at the following experimental conditions (run 11): BB concentration of 5 mg/L, treatment time of 35 min, temperature of 35 °C and Fe-OPHC concentration of 2.5 g/L. Setting 90% as the minimum acceptable adsorption value and applying Eq. 8 yielded a theoretical maximum adsorption of 99.9% at the following precise set of conditions: BB initial concentration of 6.08 mg/L, treatment time of 26.30 min, temperature of 44.79 °C and Fe-OPHC concentration of 2.27 g/L.

The statistical significance of the proposed model at 95% confidence level was confirmed by ANOVA, and the results are presented in Table 3. The F value of 123.62 ($F_{\text{model}} > F_{\text{table}} = 2.41$) suggested that the proposed model is significant and there was only a 0.01% probability that this value was a result of noise. Furthermore, the error due to the incompatibility of the mathematical form of the model is insignificant ($p > 0.05$) and thus not important for the regression model. A Pareto chart analysis (Fig. 7) was conducted to analyze the influence of each of the four process variables. Fe-OPHC concentration (X_4) and initial BB concentration (X_1) were found to have the higher contribution as indicated by their β-coefficients (p value < 0.0001) and confirmed by the Pareto chart. It is worth noting that variable X_1 showed a negative effect ($\beta_1 = -15.83$) on BB adsorption, indicating that as BB concentration increased, the process efficiency was lowered. The influence of time ($\beta_2 = 2.83$, $p < 0.05$) and temperature ($\beta_3 = 3.00$, $p < 0.02$) was very small—practically negligible when compared to the other two variables (X_1 and X_4). Fe-OPHC concentration ($\beta_4 = 36.83$) had the highest positive effect, 75% as shown in the Pareto chart. These results come in good agreement with earlier studies on BB adsorption by biomass-based adsorbents (Al-Ghouti et al. 2016; Issa et al. 2017). Figure 7 shows that the quadratic term coefficients (X_1^2 and X_4^2) were also extremely significant with small p-value (< 0.005). However, both quadratic terms have a negative effect.

Interactive effects of the process variables

Equation 8 served as the basis for drawing 3D contour plots, where the combined effect of two variables can be seen while keeping the other two variables constant. The combined influence of BB concentration–time, temperature–time and Fe-OPHC concentration–time was very low; therefore, 3D plots were only drawn for the pairs BB concentration–Fe-OPHC concentration and BB concentration–time. Figure 8a presents the combined effect of BB concentration and Fe-OPHC concentration on the adsorption process, at a treatment time of 35 min and temperature of 44 °C. At any BB concentration, as the adsorbent mass increased, so did the adsorption %, indicating a clear dependence on the adsorbent's surface area and/or functional groups. At the lowest BB concentration of 5 mg/L, a sharp, almost linear increase in adsorption % from 29.6 to 99.5% can be seen as the adsorbent concentration was raised. At the highest BB concentration of 25 mg/L, adsorption proceeded more gradually (from 0.46 to 62.6%, at 0.5 and 2.5 g/L, respectively). This demonstrated a significant degree of competition of

Table 2 Box–Behnken design and experimental results

Run no.	Variables					
	X_1: dye concentration (mg/L)	X_2: treatment time (min)	X_3: temperature (°C)	X_4: hydrochar concentration (g/L)	*Y*: adsorption (%) Experimental	predicted
1	5	10	35	1.50	75	74
2	25	10	35	1.50	37	41
3	5	60	35	1.50	81	78
4	25	60	35	1.50	45	48
5	15	35	25	0.50	15	14
6	15	35	45	0.50	19	20
7	15	35	25	2.50	88	88
8	15	35	45	2.50	92	94
9	5	35	35	0.50	22	28
10	25	35	35	0.50	6	1
11	5	35	35	2.50	98	104
12	25	35	35	2.50	77	70
13	15	10	25	1.50	57	58
14	15	60	25	1.50	64	64
15	15	10	45	1.50	65	64
16	15	60	45	1.50	71	70
17	5	35	25	1.50	77	73
18	25	35	25	1.50	38	42
19	5	35	45	1.50	84	79
20	25	35	45	1.50	44	48
21	15	10	35	0.50	15	14
22	15	60	35	0.50	18	20
23	15	10	35	2.50	89	88
24	15	60	35	2.50	93	93
25	15	35	35	1.50	65	67
26	15	35	35	1.50	68	67
27	15	35	35	1.50	70	67
28	15	35	35	1.50	66	67
29	15	35	35	1.50	67	67

BB molecules for Fe-OPHC surface pores and/or functional groups. In addition to BB concentration, the large molecular structure of the dye may have played a significant role in this phenomenon.

Figure 8b displays the effect of BB concentration and time at a constant temperature of 44 °C and Fe-OPHC concentration of 2.27 g/L. Regardless of BB concentration, it is obvious that the effect of time on adsorption is practically negligible, within the studied range. At each dye concentration, adsorption reached equilibrium in less than 10 min, thus suggesting relatively fast kinetics. This was probably due to the use of ultrasonic waves which promoted the mass and heat transfer on the adsorbent surface and at the same time enhanced the dispersion of the solute molecules. In some cases, the use of ultrasonication for longer periods may result in displacement of weakly adsorbed molecules thus reducing the adsorption efficiency. In our case, the adsorption % remained constant up to and including the 60 min treatment; therefore, this phenomenon did not occur. Without the use of ultrasonication, Masilompane et al. (2018) reported similar fast kinetics (equilibrium in < 30 min) when BB was adsorbed on a chitosan–lignin–titania nanocomposite.

Adsorption equilibrium studies

An attempt to fit the experimental data to known isothermic model equations (Langmuir and Freundlich) was performed. These isotherms are typically used to give a more detailed account of the adsorption of a solute on a solid surface; however, each has its assumptions and limitations. The Langmuir model assumes that adsorption occurs on

Table 3 Analysis of variance regression model

Source	Sum of squares	Degrees of freedom	Mean square	*F* value	*p* value Prob > *F*
Model	20,458.25	10	2045.83	123.62	< 0.0001
X_1	3008.33	1	3008.33	181.78	< 0.0001
X_2	96.33	1	96.33	5.82	0.0267
X_3	108.00	1	108.00	6.53	0.0199
X_4	16,280.33	1	16,280.33	983.76	< 0.0001
$X_1 \times X_2$	1.00	1	1.00	0.060	0.8086
$X_1 \times X_4$	6.25	1	6.25	0.38	0.5465
X_1^2	174.27	1	174.27	10.53	0.0045
X_2^2	24.25	1	24.25	1.47	0.2418
X_3^2	13.33	1	13.33	0.81	0.3814
X_4^2	885.41	1	885.41	53.50	< 0.0001
Residual	297.88	18	16.55		
Lack of fit	283.08	14	20.22	5.46	0.0566
Pure error	14.80	4	3.70		
Cor total	20,756.14	28			

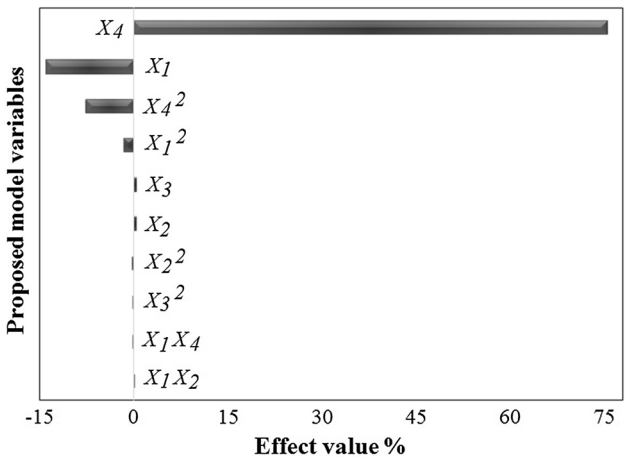

Fig. 7 Pareto chart

a homogeneous surface with equivalent adsorption sites, monolayer adsorption and no interactions between adjacent molecules. The Freundlich model addresses some of Langmuir's drawbacks (such as surface homogeneity); however, it is purely empirical and fails at high adsorbate concentrations. The details of each model isotherm have been explicitly described elsewhere (Şener et al. 2016). The values of the correlation coefficients and isotherm constants are presented in Table 4. The Langmuir model provided a better fit than the Freundlich model ($R^2 = 0.98$ compared to 0.954), suggesting a higher degree of surface rather than multilayer adsorption. This comes in good agreement with the IUPAC classification of Fe-OPHC as an essentially nonporous or macroporous material. The Langmuir isotherm also exhibited the best fit for the data of Issa et al. (2017) and Al-Gouthi et al. (2016), who investigated the adsorption of BB on acid-activated kaolinitic clay and activated wood pine, respectively. Monolayer, homogeneous adsorption of various dyes on hydrochars from different feedstocks has been frequently appeared in the literature (Parshetti et al. 2014). Masilompane et al. (2018) studied the adsorption of BB on a lignin-based nanocomposite. Contrary to this work, their data provided a much better fit to the Freundlich model, an indication of heterogeneous, multilayer adsorption. This was due to the aromatic three-dimensional polymer structure of lignin (Masilompane et al. 2018).

The equilibrium parameter R_L (also called the separation factor) is a dimensionless constant whose value indicates if the adsorption is unfavorable ($R_L > 1$), favorable ($0 < R_L < 1$) or irreversible ($R_L = 0$). It can be calculated through the following equation:

$$R_L = \frac{1}{1 + bC_0} \tag{9}$$

where b is the Langmuir constant related to the energy of adsorption and C_0 is the initial BB concentration (Masilompane et al. 2018). Figure 9 shows the R_L values as a function of the BB concentration domain used here. All values indicated favorable uptake of BB by Fe-OPHC. The irreversibility of adsorption is generally connected to the favorability of the process, thus providing a qualitative assessment of BB and Fe-OPHC interactions. Therefore, the shape of the curve revealed that adsorption became more favorable (and irreversible) at higher BB concentrations.

The favorability of the process was further supported by the Freundlich *n* value of 1.10. The adsorption capacity of 10.49 mg/g compares well to values obtained with other adsorbents, indicating stronger bonding affinity. However, the studies of BB adsorption are very few to allow for fully justified comparisons on the efficiency of each material.

Adsorption kinetics

In most cases, adsorption proceeds through a combination of mechanisms, which consist of: (1) diffusion of the adsorbate across the liquid film surrounding the adsorbent's particles, a mechanism controlled by external mass transfer, (2) adsorption through interaction with a functional group (chemisorption) or physical interaction of electrostatic nature, e.g., van der Waals forces (physisorption) and (3) intra-particle diffusion within the developed pore network of the adsorbent (Wang and Li 2007). The rate-determining mechanisms are frequently studied through the application of the pseudo-first-order, pseudo-second-order and intra-particle diffusion (IPD) models. The scientific basis and corresponding equations for each model have been thoroughly described

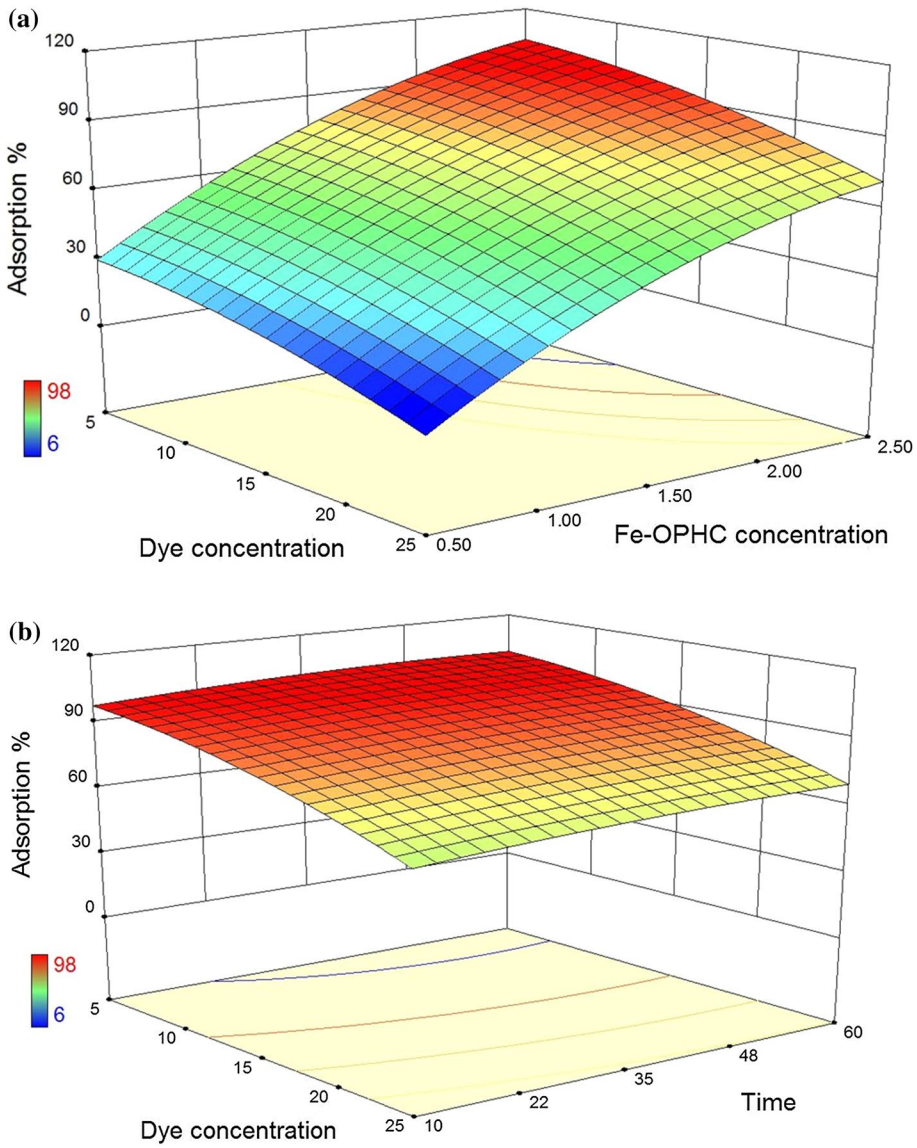

Fig. 8 **a** Effect of initial dye concentration and Fe-OPHC concentration on the adsorption of BB (time = 35 min, Temp = 44 °C) and **b** the effect of initial dye concentration and time on the adsorption of BB (Temp = 44 °C, Fe-OPHC concentration 2.27 mg/L)

Table 4 Langmuir (Langmuir 1918) and Freundlich (Freundlich 1906) isotherm parameters for this and other BB adsorption studies

Langmuir parameters			Freundlich parameters			Adsorbent	References
q_{max} (mg/g)	b	R^2	K_f	n	R^2		
10.49	0.127	0.980	0.67	1.10	0.954	Fe-modified, orange peel hydrochar	This work
1.112	0.596	n.r.	0.501	0.31	n.r.	Acid-activated kaolinitic clay	Issa et al. (2017)
15.8	0.090	0.53	8.98×10^{-5}	5.5	0.91	Chitosan–lignin–titania nanocomposite	Masilompane et al. (2018)
3.9	0.024	0.992	0.41	0.54	0.964	Activated wood pine	Al-Ghouti et al. (2016)

n.r. not reported

in the literature (Şener et al. 2016). Table 5 presents the correlation coefficients and constants for each model. The pseudo-second-order model provided a much better fit for the data, compared to the pseudo-first-order model, as indicated by the calculated q_e value and the R^2. Combined with the FTIR observations earlier, this result points out that chemical reactions (chemisorption) between BB moieties and Fe-OPHC surface groups prevailed during adsorption.

The intra-particle diffusion model describes the mass transfer resistance of the adsorbate molecules within the adsorbent's porous structure. If the plot of q (mg/g) against $t^{1/2}$ is linear and meets the axes origins, then intra-particle diffusion is the

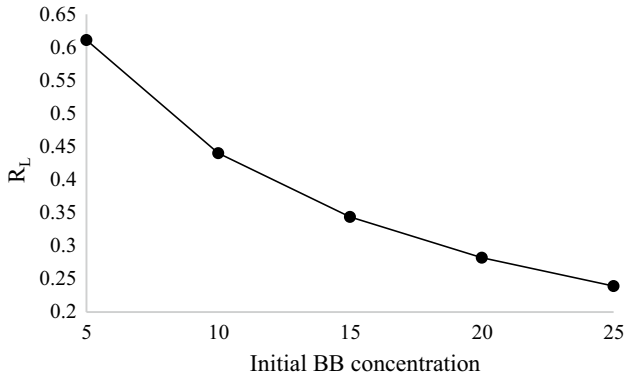

Fig. 9 Equilibrium parameter R_L as a function of BB concentration

Table 5 Values of the constants after application of the kinetic models

Kinetic model	Parameter	Value
Pseudo-first order (Lagergren 1898)	q_e, experimental (mg/g)	1.56
	q_e, calculated (mg/g)	2.11
	k_A (min^{-1})	0.190
	R^2	0.855
Pseudo-second order (Ho and McKay 1999; Blanchard et al. 1984)	q_e, calculated (mg/g)	2.01
	k_B (g/mg/min)	0.062
	R^2	0.987
IPD (Weber and Morris 1963)	k_{int} ($mg/g/min^{1/2}$)	0.27
	C (mg/g)	0.077
	R^2	0.90

rate-limiting step. In our case, the plot (not shown) exhibited multi-linearity and the C value showed that film diffusion was small but not negligible. Therefore, intra-particle diffusion was not the rate-determining step, a conclusion that is supported by the earlier characterization of Fe-OPHC as an essentially non-porous or macroporous material. Zhu et al. prepared magnetic hydrochar from *Salix psammophila* and investigated the adsorption of malachite green (MG). Although the composite adsorbent attained a highly developed porous structure after activation, their data followed the pseudo-second-order model and they concluded that intra-particle diffusion did not exclusively control MG adsorption (Zhu et al. 2014).

Conclusion

As part of a waste management scenario, hydrochar was prepared from orange peel residues and subsequently embedded with magnetite nanoparticles. It was demonstrated that hydrothermal carbonization of orange peel is a simple, safe and environmentally friendly process that can be used to convert orange peel and other high moisture organic waste to added-value products. Furthermore, hydrochar production may follow other biomass exploitation options, such as extraction and isolation of essential oils and/or nutrients. Overall, Fe-OPHC showed a promising behavior in adsorption of Brilliant Black. Maximum adsorption of 98% was obtained at initial dye concentration of 5 mg/L, contact time of 35 min, temperature of 35 °C and adsorbent dosage 2.5 g/L. Future work involves tests with multiple dye solutions as well as solutions of heavy metals and other inorganic contaminants. However, before any larger-scale applications of hydrochars can be materialized, the potential toxicity and environmental impact of the HTC wastewater should be addressed. There is still a significant research gap on the full characterization of HTC wastewater and gaseous products from various biomasses and the correlation of the production of specific organics to the initial biomass properties, process temperature and time.

Acknowledgements This work has been supported by the Research Fund of Aksaray University—Project Number 2017-042.

Compliance with ethical standards

Conflict of interest The authors declare that they have no conflict of interest.

References

Ahn T, Kim JH, Yang HM, Lee JW, Kim JD (2012) Formation pathways of magnetite nanoparticles by coprecipitation method. J Phys Chem C 116:6069–6076. https://doi.org/10.1021/jp211843g

Al-Ghouti MA, Issa AA, Al-Saqarat BS, Al-Reyahi AY, Al-Degs YS (2016) Multivariate analysis of competitive adsorption of food dyes by activated pine wood. Desalin Water Treat 57:27651–27662. https://doi.org/10.1080/19443994.2016.1174742

Aliramaji S, Zamanian A, Sohrabijam Z (2015) Characterization and synthesis of magnetite nanoparticles by innovative sonochemical method. Procedia Mater Sci 11:265–269. https://doi.org/10.1016/j.mspro.2015.11.022

Al-Othman ZA, Ali R, Naushad M (2012) Hexavalent chromium removal from aqueous medium by activated carbon prepared from peanut shell: adsorption kinetics, equilibrium and thermodynamic studies. Chem Eng J 184:238–247. https://doi.org/10.1016/j.cej.2012.01.048

Anastopoulos I, Kyzas GZ (2014) Agricultural peels for dye adsorption: a review of recent literature. J Mol Liq 200:381–389. https://doi.org/10.1016/j.molliq.2014.11.006

Bagheri AR, Ghaedi M, Asfaram A, Bazrafshan AA, Jannesar R (2017) Comparative study on ultrasonic assisted adsorption of dyes from single system onto Fe_3O_4 magnetite nanoparticles loaded on activated carbon: experimental design methodology. Ultrason Sonochem 34:294–304. https://doi.org/10.1016/j.ultsonch.2016.05.047

Blanchard G, Maunaye M, Martin G (1984) Removal of heavy metals from waters by means of natural zeolites. Water Res 18(12):1501–1507. https://doi.org/10.1016/0043-1354(84)90124-6

Daneshvar E, Vazirzadeh A, Niazi A, Kousha M, Naushad M, Bhatnagar A (2017) Desorption of Methylene blue dye from brown macroalga: effects of operating parameters, isotherm study and kinetic modeling. J Clean Prod 152:443–453. https://doi.org/10.1016/j.jclepro.2017.03.119

De Lange MF, Vlugt TJH, Gascon J, Kapteijn F (2014) Adsorptive characterization of porous solids: error analysis guides the way. Microporous Mesoporous Mater 200:199–215. https://doi.org/10.1016/j.micromeso.2014.08.048

Deepa K, Prasad C, Jyothi N, Naushad M, Rajendran S, Karlapudi S, Kumar SH (2018) Adsorptive removal of Pb(II) metal from aqueous medium using biogenically synthesized and magnetically recoverable core-shell structured AM@ Cu/Fe3O4 nano composite. Desalin Water Treat 111:278–285. https://doi.org/10.5004/dwt.2018.22200

European Food Safety Authority (2010) Scientific Opinion on the re-evaluation of Brilliant Blue FCF (E 133) as a food additive. EFSA J 8:1853. https://doi.org/10.2903/j.efsa.2010.1853

European Food Safety Authority (2015) Refined exposure assessment for Brilliant Black BN (E 151). EFSA J 13:3960. https://doi.org/10.2903/j.efsa.2015.3960

European Biochar Foundation (EBC) (2018) Guidelines for a sustainable production of biochar v4.5E, Eur. Biochar Found. v4.5. European Biochar Foundation, Arbaz, pp 1–22. https://doi.org/10.13140/rg.2.1.4658.7043

Fang J, Gao B, Zimmerman AR, Ro KS, Chen J (2016) Physically (CO_2) activated hydrochars from hickory and peanut hull: preparation, characterization, and sorption of methylene blue, lead, copper, and cadmium. RSC Adv 6:24906–24911. https://doi.org/10.1039/C6RA01644H

Fernandez ME, Ledesma B, Román S, Bonelli PR, Cukierman AL (2015) Development and characterization of activated hydrochars from orange peels as potential adsorbents for emerging organic contaminants. Bioresour Technol 183:221–228. https://doi.org/10.1016/j.biortech.2015.02.035

Freundlich H (1906) Over the adsorption in solution. J Physical Chem 57:385–470

Gnanasekaran L, Hemamalini R, Rajendran S, Qin J, Yola ML, Atar N, Gracia F (2019) Nanosized Fe_3O_4 incorporated on a TiO_2 surface for the enhanced photocatalytic degradation of organic pollutants. J Mol Liq 287:110967. https://doi.org/10.1016/j.molliq.2019.110967

Guo S, Dong X, Wu T, Zhu C (2016a) Influence of reaction conditions and feedstock on hydrochar properties. Energy Convers Manag 123:95–103. https://doi.org/10.1016/j.enconman.2016.06.029

Guo X, Dong H, Yang C, Zhang Q, Liao C, Zha F et al (2016b) Application of goethite modified biochar for tylosin removal from aqueous solution. Colloids Surf A Physicochem Eng Asp 502:81–88. https://doi.org/10.1016/j.colsurfa.2016.05.015

Han L, Sun H, Ro KS, Sun K, Libra JA, Xing B (2017) Removal of antimony (III) and cadmium (II) from aqueous solution using animal manure-derived hydrochars and pyrochars. Bioresour Technol 234:77–85. https://doi.org/10.1016/j.biortech.2017.02.130

Ho YS, McKay G (1999) Pseudo-second order model for sorption processes. Process Biochem 34:451–465. https://doi.org/10.1016/S0032-9592(98)00112-5

Holkar CR, Jadhav AJ, Pinjari DV, Mahamuni NM, Pandit AB (2016) A critical review on textile wastewater treatments: possible approaches. J Environ Manag 182:351–366. https://doi.org/10.1016/j.jenvman.2016.07.090

Issa AA, Abdel-Halim HM, Al-Degs YS, Al-Masri HA (2017) Application of multivariate calibration for studying competitive adsorption of two problematic colorants on acid-activated-kaolinitic clay. Res Chem Intermed 43:523–544. https://doi.org/10.1007/s11164-016-2638-0

Kalderis D, Kotti MS, Méndez A, Gascó G (2014) Characterization of hydrochars produced by hydrothermal carbonization of rice husk. Solid Earth 5:477–483. https://doi.org/10.5194/se-5-477-2014

Kamboh MA, Yilmaz M (2013) Synthesis of N-methylglucamine functionalized calix[4]arene based magnetic sporopollenin for the removal of boron from aqueous environment. Desalination 310:67–74. https://doi.org/10.1016/j.desal.2012.10.034

Khataee A, Kayan B, Kalderis D, Karimi A, Akay S, Konsolakis M (2017) Ultrasound-assisted removal of Acid Red 17 using nanosized Fe_3O_4-loaded coffee waste hydrochar. Ultrason Sonochem 35:72–80. https://doi.org/10.1016/j.ultsonch.2016.09.004

Kulaksiz E, Gözmen B, Kayan B, Kalderis D (2017) Adsorption of malachite green on Fe-modified biochar: influencing factors and process optimization. Desalin Water Treat. https://doi.org/10.5004/dwt.2017.20601

Lagergren S (1898) About the theory of so-called adsorption of soluble substances. K Sven Vetenskapsakad Handl 24:1–39

Langmuir I (1918) The adsorption of gases on plane surfaces of glass, mica and platinum. J Am Chem Soc 40:1362–1403. https://doi.org/10.1021/ja02242a004

Libra JA, Ro KS, Kammann C, Funke A, Berge ND, Neubauer Y, Titirici M-M, Fühner C, Bens O, Kern J, Emmerich K-H (2011) Hydrothermal carbonization of biomass residuals: a comparative review of the chemistry, processes and applications of wet and dry pyrolysis. Biofuels 2(1):89–124. https://doi.org/10.4155/BFS.10.81

Masilompane TM, Chaukura N, Mishra SB, Mishra AK (2018) Chitosan-lignin-titania nanocomposites for the removal of brilliant black dye from aqueous solution. Int J Biol Macromol 120:1659–1666. https://doi.org/10.1016/j.ijbiomac.2018.09.129

Moeser GD, Roach KA, Green WH, Laibinis PE, Hatton TA (2002) Water-based magnetic fluids as extractants for synthetic organic compounds. Ind Eng Chem Res 41:4739–4749. https://doi.org/10.1021/ie0202118

Naushad M (2014) Surfactant assisted nano-composite cation exchanger: development, characterization and applications for the removal of toxic Pb^{2+} from aqueous medium. Chem Eng J 235:100–108. https://doi.org/10.1016/j.cej.2013.09.013

Naushad M, Al-Othman ZA (2015) Separation of toxic Pb^{2+} metal from aqueous solution using strongly acidic cation-exchange resin: analytical applications for the removal of metal ions from pharmaceutical formulation. Desalin Water Treat 53:2158–2166. https://doi.org/10.1080/19443994.2013.862744

Naushad M, Al-Othman ZA, Rabiul Awual M, Alfadul SM, Ahamad T (2016a) Adsorption of rose Bengal dye from aqueous solution by amberlite Ira-938 resin: kinetics, isotherms, and thermodynamic studies. Desalin Water Treat 57:13527–13533. https://doi.org/10.1080/19443994.2015.1060169

Naushad M, Vasudevan S, Sharma G, Kumar A, Al-Othman Z (2016b) Adsorption kinetics, isotherms, and thermodynamic studies for Hg^{2+} adsorption from aqueous medium using alizarin red-S-loaded amberlite IRA-400 resin. Desalin Water Treat 57:18551–18559. https://doi.org/10.1080/19443994.2015.1090914

Naushad M, Ahamad T, Sharma G, Al-Muhtaseb AH, Albadarin AB, Alam MM, Al-Othman ZA, Alshehri SM, Ghfar AA (2016c) Synthesis and characterization of a new starch/SnO_2 nanocomposite for efficient adsorption of toxic Hg^{2+} metal ion. Chem Eng J 300:306–316. https://doi.org/10.1016/j.cej.2016.04.084

Naushad M, Ahamad T, Al-Maswari BM, Abdullah Alqadami A, Alshehri SM (2017) Nickel ferrite bearing nitrogen-doped mesoporous carbon as efficient adsorbent for the removal of highly toxic metal ion from aqueous medium. Chem Eng J 330:1351–1360. https://doi.org/10.1016/j.cej.2017.08.079

Parshetti GK, Chowdhury S, Balasubramanian R (2014) Hydrothermal conversion of urban food waste to chars for removal of textile dyes

from contaminated waters. Bioresour Technol 161:310–319. https://doi.org/10.1016/j.biortech.2014.03.087

Qin J, Yang C, Cao M, Zhang X, Rajendran S, Limpanart S, Ma M, Liu R (2017) Two-dimensional porous sheet-like carbon-doped ZnO/g-C_3N_4 nanocomposite with high visible-light photocatalytic performance. Mater Lett 189:156–159. https://doi.org/10.1016/j.matlet.2016.12.007

Quesada-Plata F, Ruiz-Rosas R, Morallón E, Cazorla-Amorós D (2016) Activated carbons prepared through H_3PO_4-assisted hydrothermal carbonisation from biomass wastes: porous texture and electrochemical performance. ChemPlusChem 81:1349–1359. https://doi.org/10.1002/cplu.201600412

Reza MT, Andert J, Wirth B, Busch D, Pielert J, Lynam JG et al (2014) Hydrothermal carbonization of biomass for energy and crop production. Appl Bioenergy 1:11–29. https://doi.org/10.2478/apbi-2014-0001

Román S, Libra J, Berge N, Sabio E, Ro K, Li L, Ledesma B, Álvarez A, Bae S (2015) Hydrothermal carbonization: modeling, final properties design and applications: a review. Renew Sustain Energy Rev 45:359–378. https://doi.org/10.3390/en11010216

Román S, Ledesma B, Álvarez-Murillo A, Sabio E, González JF, González CM (2016) Production of cost-effective mesoporous materials from prawn shell hydrocarbonization. Nanoscale Res Lett. https://doi.org/10.1186/s11671-016-1634-z

Rovira J, Domingo JL (2019) Human health risks due to exposure to inorganic and organic chemicals from textiles: a review. Environ Res 168:62–69. https://doi.org/10.1016/j.envres.2018.09.027

Saravanan R, Aviles J, Gracia F, Mosquera E, Gupta VK (2018) Crystallinity and lowering band gap induced visible light photocatalytic activity of TiO_2/CS (Chitosan) nanocomposites. Int J Biol Macromol 109:1239–1245. https://doi.org/10.1016/j.ijbiomac.2017.11.125

Şener M, Kayan B, Akay S, Gözmen B, Kalderis D (2016) Fe-modified sporopollenin as a composite biosorbent for the removal of Pb^{2+} from aqueous solutions. Desalin Water Treat 3994:1–19. https://doi.org/10.1080/19443994.2016.1182449

Sharma G, Naushad M, Pathania D, Mittal A, El-Desoky G (2015) Modification of *Hibiscus cannabinus* fiber by graft copolymerization: application for dye removal. Desalin Water Treat 54:3114–3121. https://doi.org/10.1080/19443994.2014.904822

Sharma G, Naushad M, Kumar A, Rana S, Sharma S, Bhatnagar A, Stadler FJ, Ghfar AA, Khan MR (2017) Efficient removal of coomassie brilliant blue R-250 dye using starch/poly(alginic acid-cl-acrylamide) nanohydrogel. Process Saf Environ 109:301–310. https://doi.org/10.1016/j.psep.2017.04.011

Simsir H, Eltugral N, Karagoz S (2017) Hydrothermal carbonization for the preparation of hydrochars from glucose, cellulose, chitin, chitosan and wood chips via low-temperature and their characterization. Bioresour Technol 246:82–87. https://doi.org/10.1016/j.biortech.2017.07.018

Sivarajasekar N, Baskar R (2015) Agriculture waste biomass valorisation for cationic dyes sequestration: a concise review. J Chem Pharm Res 7:737–748

Takaya CA, Fletcher LA, Singh S, Anyikude KU, Ross AB (2016) Phosphate and ammonium sorption capacity of biochar and hydrochar from different wastes. Chemosphere 145:518–527. https://doi.org/10.1016/j.chemosphere.2015.11.052

Tang Z, Deng Y, Luo T, Sheng Xu Y, Min Zhu N (2016) Enhanced removal of Pb(II) by supported nanoscale Ni/Fe on hydrochar derived from biogas residues. Chem Eng J 292:224–232. https://doi.org/10.1016/j.cej.2016.01.113

Thommes M (2010) Physical adsorption characterization of nanoporous materials. ChemIngTech 82:1059–1073. https://doi.org/10.1002/cite.201000064

Unur E (2013) Functional nanoporous carbons from hydrothermally treated biomass for environmental purification. Microporous Mesoporous Mater 168:92–101. https://doi.org/10.1016/j.micromeso.2012.09.027

Wang S, Li H (2007) Kinetic modelling and mechanism of dye adsorption on unburned carbon. Dye Pigment 72:308–314. https://doi.org/10.1016/j.dyepig.2005.09.005

Wang T, Zhai Y, Zhu Y, Li C, Zeng G (2018) A review of the hydrothermal carbonization of biomass waste for hydrochar formation: process conditions, fundamentals, and physicochemical properties. Renew Sustain Energy Rev 90:223–247. https://doi.org/10.1016/j.rser.2018.03.071

Weber WJ, Morris JC (1963) Kinetics of adsorption on carbon from solution. J Sanit Eng Div 89(2):31–60

Zhou N, Chen H, Xi J, Yao D, Zhou Z, Tian Y et al (2017) Biochars with excellent Pb(II) adsorption property produced from fresh and dehydrated banana peels via hydrothermal carbonization. Bioresour Technol 232:204–210. https://doi.org/10.1016/j.biortech.2017.01.074

Zhou Y, Lu J, Zhou Y, Liu Y (2019) Recent advances for dyes removal using novel adsorbents: a review. Environ Pollut 252:352–365. https://doi.org/10.1016/j.envpol.2019.05.072

Zhu X, Liu Y, Zhou C, Zhang S, Chen J (2014) Novel and high-performance magnetic carbon composite prepared from waste hydrochar for dye removal. ACS Sustain Chem Eng 2:969–977. https://doi.org/10.1021/sc400547y